ChemPubSoc Europe

DOI: 10.1002/celc.201901896

CHEMELECTROCHEM Articles

Titanium as a Substrate for Three-Dimensional Hybrid Electrodes for Vanadium Redox Flow Battery Applications

Xubin Lu,[a] Fan Li,[b] Matthias Steimecke,[a] Muhammad Tariq,[c] Mark Hartmann,[a] and Michael Bron*[a]

Titanium, either in the form of a Ti foil or in form of a Ti mesh, was used as a novel substrate to grow nitrogen-doped carbon nanotubes (NCNTs) through chemical vapor deposition at moderate temperatures over electrodeposited iron particles. The thus-prepared high-surface-area electrodes were characterized by scanning electron microscopy (SEM), Raman spectroscopy, and X-ray photoelectron spectroscopy (XPS). The electrochemical performance towards the V(IV)/V(V) redox couple was investigated by cyclic voltammetry. The parameters for iron particle electrodeposition were adjusted towards high and uniform substrate coverage. Nanotube growth from acetonitrile at moderate temperatures (600 °C) led to N-containing CNTs with a high amount of graphitic nitrogen. NCNTs grown over Ti substrates provide promising performances towards the V(IV)/V(V) as well as the V(III)/V(IV) redox pair. In general, the results of this study show that Ti might be a suitable electrocatalyst substrate for various applications in electrochemical energy conversion.

1. Introduction

The all-vanadium redox flow battery (VRFB) is considered one of the most promising solutions for stationary storage of fluctuating renewable energy, which is based on its advantageous characteristics including high and flexible capacity, high energy efficiency, and long cycle life.[1] The energy in VRFBs is stored using redox reactions of dissolved species, and the relevant redox pair in the positive electrolyte solution is VO^{2+}/VO_2^{+} and in the negative one V^{2+}/V^{3+},[2] respectively. Unlike other types of redox flow batteries, the VRFB only involves redox reactions with one single metal with various valence states, which prevents a fast electrolyte degradation from cross-contamination of the solutions of both half cells.

It is obvious that the electrodes play a crucial role in catalysing redox reactions involved in electrochemical energy conversion.[3] While the iR-drop (Ohmic overvoltage) and the depletion of active redox species (mass-transport overvoltage) only evolve at high electrical currents, kinetic overvoltage is a detrimental energy barrier through the whole current range of a realistic VRFB. It already emerges at low currents and typically has a logarithmical progression (Tafel-slope) in a *U* vs. *I* diagram (polarization curve). Distinct influences of non-Ohmic overvoltages (ASR-free voltage) in real VRFB have been reported,[4] where the kinetic overvoltage shows a logarithmic progression below ~200 mA cm^{-2} and increases approximately linear above ~200 mA cm^{-2} and catalytically active electrodes are required to overcome the resulting efficiency losses.

For VRFBs, carbon-based electrodes based on graphite felts[5] meet most requirements including high electrical conductivity (at least under compression), availability and price.[6] However, it was also shown that this standard electrode material (carbon felt/carbon nonwoven) has to be activated in order to provide an acceptable catalytic activity for vanadium ion redox conversion,[7] and even in this case further improvement is desired to overcome kinetic limitations, as detailed above. Thus, recent research focusses on the investigation of catalytically active carbon material, such as carbon fibres,[8] carbon nanotubes,[9] mesoporous carbon,[1b,10] carbon nanospheres,[11] and more.

Besides the active electrode material itself, the substrate electrode onto which this material is deposited also requires attention. Requirements are in particular long-term (electro) chemical stability, appropriate flow-through properties, high conductivity as well as high mechanical stability (high compression resistance against clamping forces). The compression resistance strongly correlates with the void/pore morphology (macro-porosity and/or flow channels) of the flow-through electrode, however, is inversely related to the area specific resistance (ASR).[12] With carbon felts these are critical issues due to their high compressibility leading to increased flow-through resistance under high clamping forces, which in turn are necessary to reduce the ASR. However, non-carbon electrodes potentially are superior regarding these nontrivial dependencies if they could provide superior mechanical properties[13] including high compression resistance. In this work, titanium (Ti), which is electrochemically stable under the strongly corrosive

[a] X. Lu, Dr. M. Steimecke, M. Hartmann, Prof. Dr. M. Bron
Institut für Chemie, Technische Chemie I
Martin-Luther-Universität Halle-Wittenberg
von-Danckelmann-Platz 4, 06120 Halle (Saale) (Germany)
E-mail: michael.bron@chemie.uni-halle.de
[b] Dr. F. Li
Max-Planck-Institut für Mikrostrukturphysik
Weinberg 2, D-06120 Halle (Saale) (Germany)
[c] M. Tariq
Institut für Physik, FG Polymerphysik
Martin-Luther-Universität Halle-Wittenberg
Von-Danckelmann-Platz 3, D-06120 Halle (Saale) (Germany)

environment of a VRFB (as compared to e.g. Ni or Fe) and provides very good electrical conductivity, has been used as substrate for nitrogen-doped carbon nanotubes (NCNTs). This study demonstrates for the first time an electrode for the positive half-cell reaction of a VRFB, consisting of a 3-dimensional nitrogen-doped carbon nanotube (NCNTs) surface layer with a dimensionally stable anode substrate (DSA titanium core). From a more general point of view, this study provides the prospective of electrodes with tuneable catalytic activity and surface area,[14] stable void morphologies (e.g. for slotted flow channels) and low ASR due to a high metallic compression resistance against clamping forces.

To provide good electrical contact and adhesion, the NCNTs were directly grown onto the substrate using chemical vapour deposition (CVD) yielding high-surface-area composite electrodes with tuneable properties.[15]

Two different substrates were chosen, i.e. Ti foil and Ti mesh. The thus obtained composite electrodes demonstrate good activity for vanadium ion redox reactions and might be suitable for other devices for electrochemical energy conversion as well.

2. Results and Discussion

Iron particles were potentiostatically deposited onto both Ti foil and Ti mesh using a potential sequence as shown in Figure 1(a). The classical double pulse deposition approach using a short nucleation pulse to form nuclei on the substrate surface and a longer growth pulse to grow the nuclei into clusters did not yield uniform and homogeneous coverage of the Ti surfaces, thus a considerably long initial polarisation ($t_1 = 60–120$ s) to a rather negative potential was necessary. We tentatively attrib-

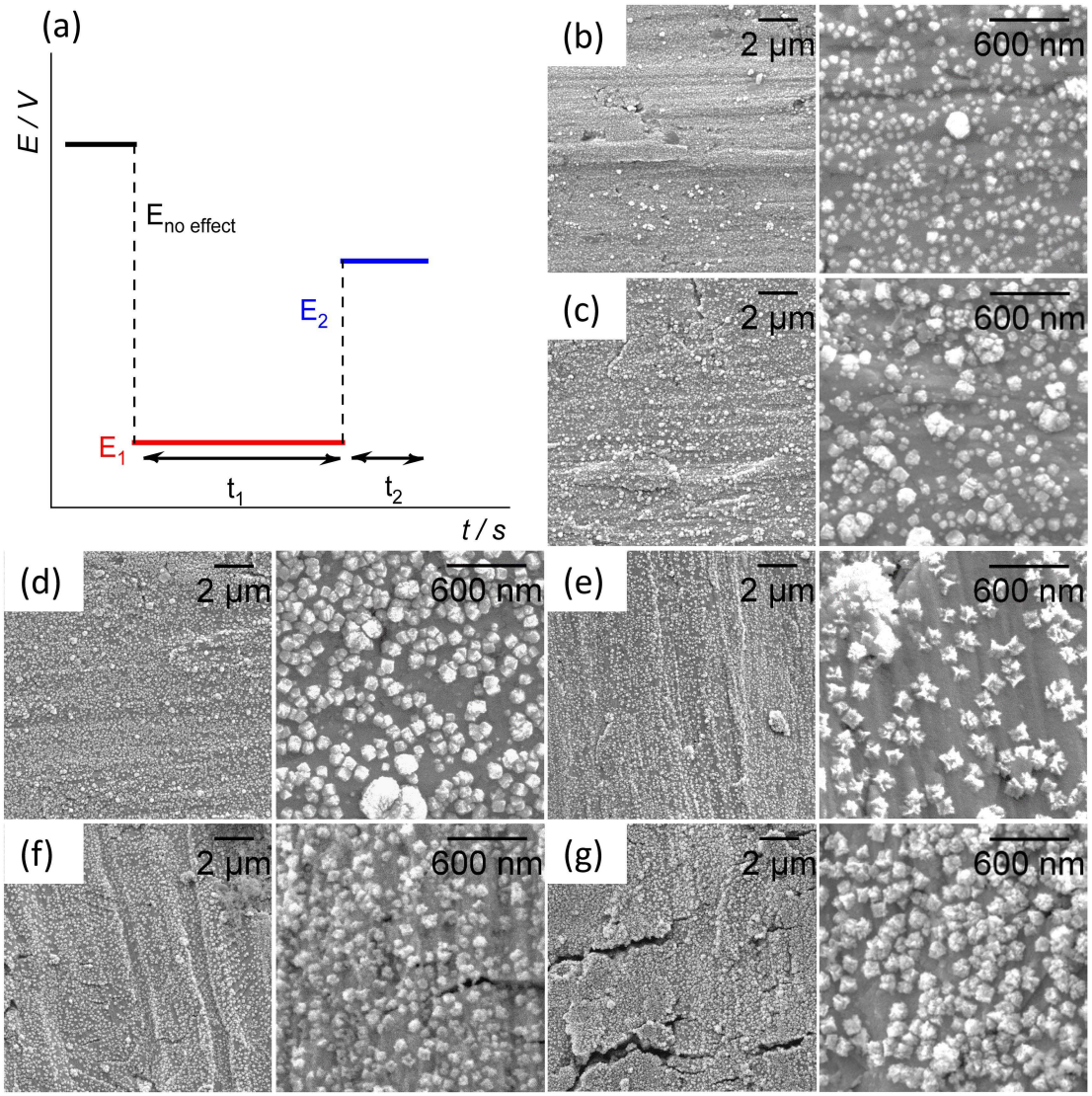

Figure 1. Electrodeposition parameters and SEM images of Fe particles on Ti substrates. a) Schematic representation of the electrodeposition potential profile. $E_1 = -3$ V, $E_2 = -0.7$ V, t_1: nucleation time, t_2: growth time. SEM images of as-deposited Fe particles on: b–d) Ti foil, and e–g) Ti mesh, showing the effect of t_1: b, e) 60 s, c, f) 90 s and d, g) 120 s, $t_2 = 10$ s.

ute this to the presence of a thin oxide layer covering the Ti substrate (see below). After optimising the Fe deposition times, dense coverage of Fe particles on the Ti substrate was obtained, as shown in Figure 1. Further optimisation of the deposition procedure (e.g., also varying the deposition potential etc.) was beyond the scope of this paper. The images obtained with SEM shown in Figures 1 (b–d) for Ti foil and (e–g) for Ti mesh demonstrate the effect of varying t_1 on the dispersion and size of the Fe particles when t_2 was set to 10 s. Increasing coverage as well as particle sizes are observed with increasing deposition time. When the t_1 is maintained for 60 s, still incomplete coverage may be observed in particular in case of the Ti mesh (Figure 1e), while at deposition times of $t_1 = 120$ s the individual particles start to coalesce to larger ones (Figures 1d and 1 g). Homogeneous and rather uniform as well as individual Fe particles are detected at $t_1 = 90$ s in both cases (Figures 1c and 1 f).

NCNTs were CVD-grown over electrodeposited iron particles as detailed in the experimental section and were characterized with SEM/EDX, Raman spectroscopy and XPS. SEM images of the grown NCNTs under variation of electrodeposition and growth time are shown in Figure 2. From Figures 2a–c (Ti foil) and Figures 2d–f (Ti mesh), one can see that dense NCNT layers are grown over the samples prepared with varying deposition time t_1 (2a,d: 60 s, 2b,f: 90 s, 2c,g: 120 s). However, comparing the inset of Figure 2d with those of Figures 2e and f, it appears that after $t_1 = 60$ s the NCNT layer is still rather open (compare areas within the circles in Figure 2d) and full and dense coverage is only obtained after $t_1 = 90$ s, indicating that the coverage with Fe particles is insufficient at $t_1 = 60$ s (although the differences are small), in agreement with Figures 1(e). Both Ti foil and Ti mesh are completely covered with the NCNTs when t_1 is increased to 90 s (Figures 2b,f). Combining the results from Figure 1 and Figure 2, $t_1 = 90$ s has been chosen as

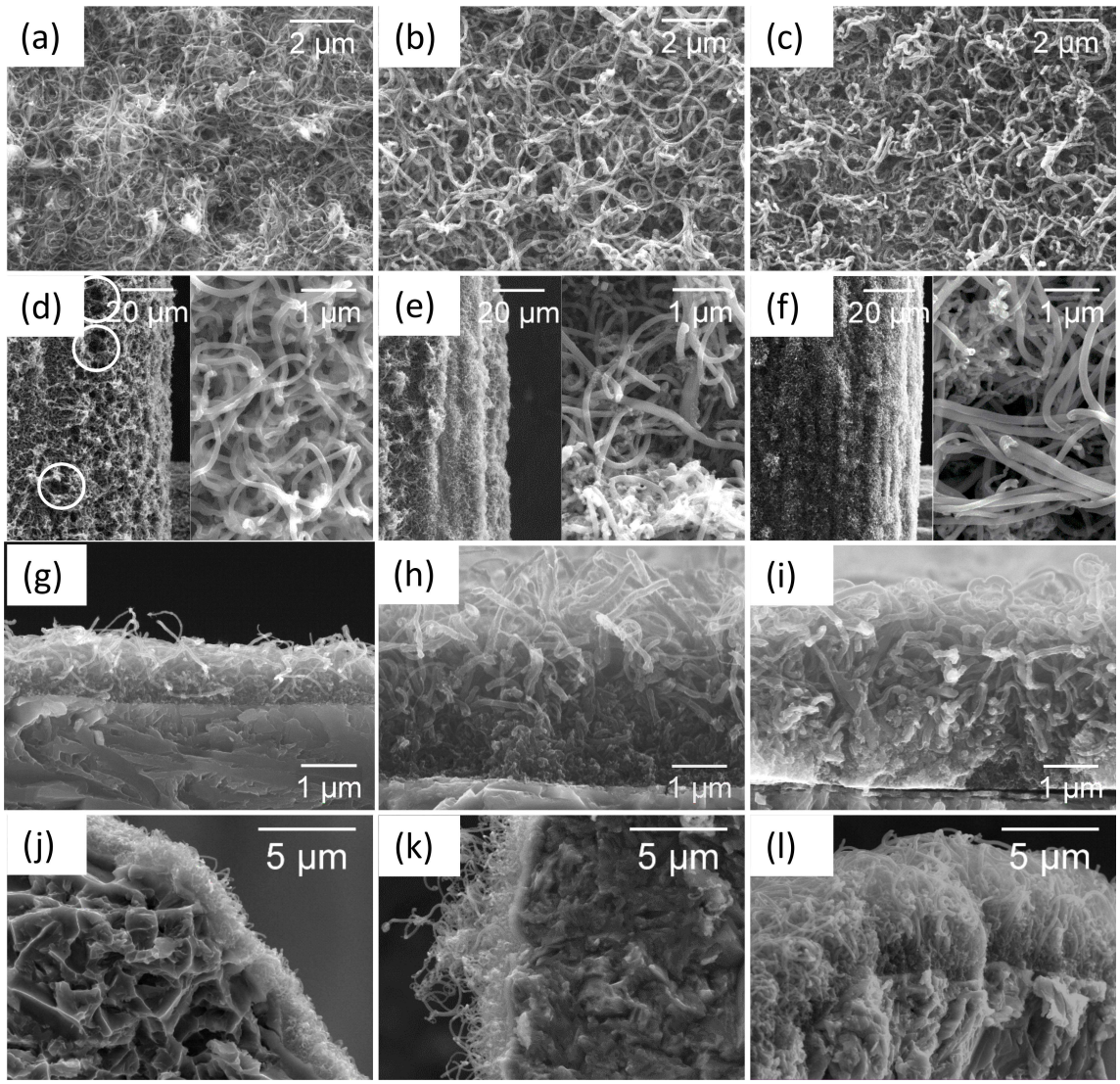

Figure 2. SEM micrographs of NCNTs on: a–c) Ti foil, and d–f) Ti mesh showing the effect of t_1. a,d) $t_1 = 60$ s, b,e) $t_1 = 90$ s, and c,f) $t_1 = 120$ s, $t_2 = 10$ s. The growth time (t_G) is 90 min, the substrate temperature is 600 °C. SEM micrographs of NCNTs on: g–i) Ti foil, and j–l) Ti mesh showing the effect of t_G. g,j) $t_G = 60$ min, h,k) $t_G = 90$ min, and i,l) $t_G = 120$ min (Fe electrodeposition in all cases with $t_1 = 90$ s and $t_2 = 10$ s). Circles in Figure 2d indicate voids in the nanotube layer.

deposition time for further experiments, as the homogeneous Fe deposition leads to a homogeneous but still open 3-dimensional NCNT layer. To further tune the properties of the NCNT layers on the Ti substrates, the growth time (t_G) has been varied, using 60, 90 and 120 min. Results of NCNTs grown over Ti foil are shown in Figures 2 (g–i), while those for the Ti mesh are displayed in Figures 2 (j–l). As expected, the thickness of the layers increases with growth time on both substrates.

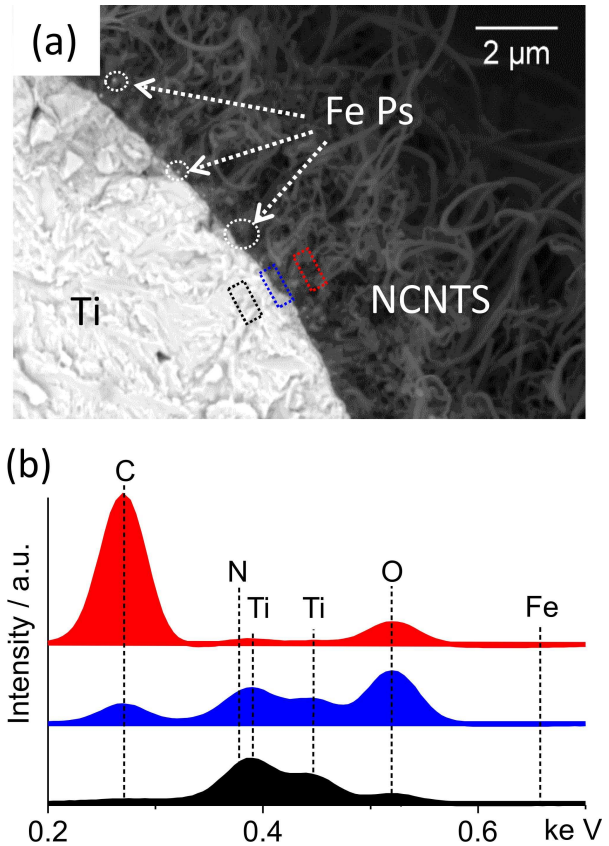

Figure 3. a) SEM-BSE micrographs of as-grown NCNTs on Ti mesh. b) EDX analysis along area marked in black, blue, and red in Figure 3a. $t_1 = 90$ s, $t_2 = 10$ s. $t_G = 90$ min, $T_S = 600\,^{\circ}C$.

When carbon nanomaterials are grown on Cu,[16] Ni,[17] or Fe[18] by CVD, a metal-C layer is commonly detected which is attributed to the dissolution of C into these metals leading to the formation of a new thin interface layer under various temperatures. To gain deeper insight into the interface between NCNT layer and substrate, detailed SEM/energy-dispersive X-ray spectroscopy (EDX) measurements were carried out. The back-scattered electrons (BSE) cross-view SEM images of the interface between Ti mesh and NCNTs are shown in Figure 3a. EDX measured on the Ti mesh (black), the interface (blue) and the NCNTs (red) is displayed in Figure 3b with the investigated areas marked in the figure with the same colors. The spectra show peaks corresponding to carbon at 0.27 keV, nitrogen at 0.38 keV, Ti at 0.39 and 0.45 keV, and oxygen at 0.52 keV. Iron (at 0.66 keV) however is below the limit of detection. Obviously, the Ti mesh essentially consists of Ti and a small amount of O, while the interface seems to consist mainly of TiO_2 as concluded from the intense oxygen signal. The NCNT layer demonstrates the expected signals of C and N, while also O can be found (see also below, XPS analysis).

To evaluate the structural properties of carbon materials, often Raman spectroscopy is the method of choice. Typically, the D, G, and 2D bands at ca. 1341, 1588, and 2682 cm^{-1} [19,20] are analyzed and the intensity ratio of the D to G band (I_D/I_G) is commonly used as an estimate of the quality of sp^2 carbon material, e.g. NCNTs. The respective Raman spectra shown in Figure 4a indicate that the quality/amount of defects in NCNTs grown on Ti-foil and Ti-mesh, respectively, is comparable, with only a minor influence of the substrate on their properties. Furthermore, to evaluate the homogeneity of the grown NCNT layer, Raman mappings have been performed. Figure 4b visualizes a statistical evaluation of the Raman mapping experiment with mean value as solid line and standard deviation as grey shadow from 178 single spectra. The mean I_D/I_G intensity is about 0.86 ± 0.02 for NCNTs grown on a Ti foil ($t_1 = 90$ s and $t_G = 90$ min) with very low standard deviation, implying that the

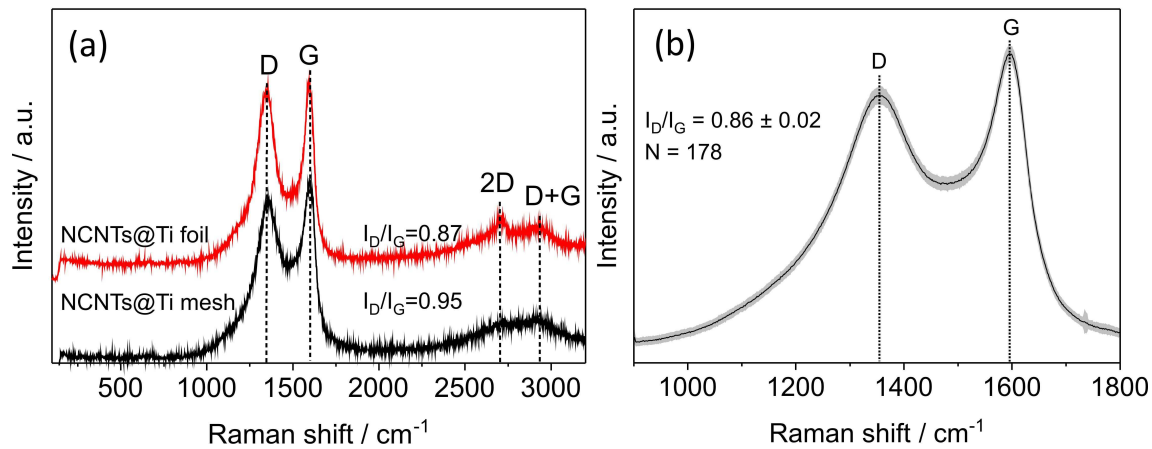

Figure 4. a) Raman spectra of NCNTs on Ti foil and Ti mesh after testing electrochemical performance. b) Statistical evaluation of the Raman mapping experiment with mean value and standard deviation (grey shadow) from 178 single spectra of NCNTs on Ti foil. $t_1 = 90$ s, $t_2 = 10$ s. $t_G = 90$ min, $T_S = 600\,^{\circ}C$.

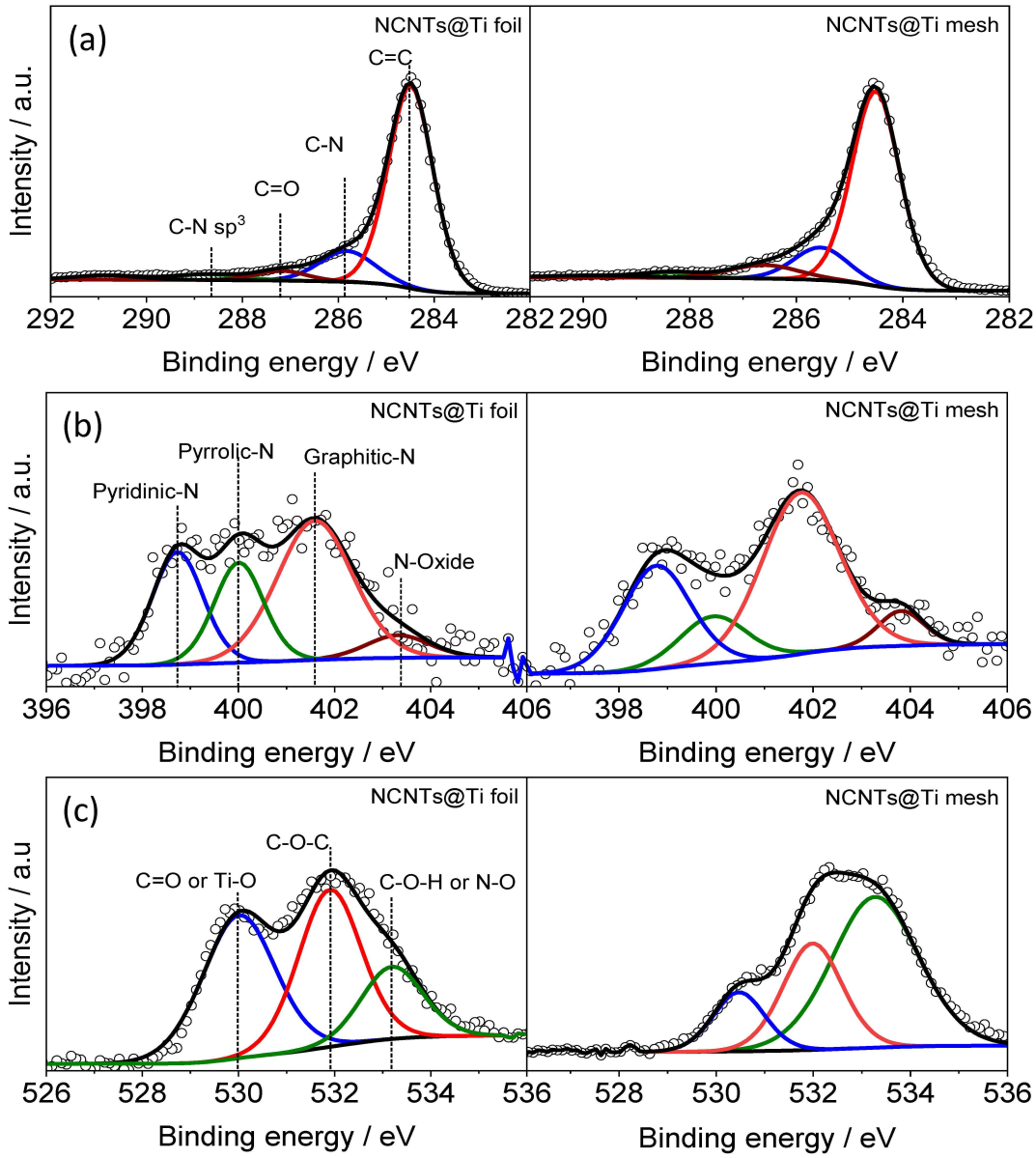

Figure 5. XPS high-resolution spectra of NCNTs on Ti foil and Ti mesh. a) C 1 s, b) N 1 s, and c) O 1 $t_1 = 90$ s, $t_2 = 10$ s, $t_G = 90$ min, $T_S = 600$ °C.

NCNTs are grown rather homogeneously on the Ti foil. Furthermore, in the Raman spectra of Figure 4a the characteristic radial breathing model (RBM) at ca. 160–290 cm^{-1}[21,22] is not visible, indicating that the NCNTs indeed are multi-walled, as expected.

Table 1. Surface atomic composition of the NCNTs derived from XPS for characteristic binding energies of C 1s (285 eV), O 1s (532 eV), N 1s (402 eV), Ti 2p (459 eV) and Fe 2p (714 eV).

	C 1 s [at%]	O 1 s [at%]	N 1 s [at%]	Ti 2p [at%]	Fe [at%]
Ti foil	94.1	2.1	3.8	< LOD[a]	< LOD[a]
Ti mesh	93.6	3.0	3.4	< LOD[a]	< LOD[a]

[a] LOD-limit of detection, here ~0.5 at%

X-ray photoelectron spectroscopy was used to analyze the chemical composition of the NCNTs grown over Ti foil and Ti mesh. The XP survey spectra show the C 1s peak at 285 eV, the O 1s peak at 532 eV, the N 1s peak at 402 eV, and Ti 2p peak at 459 eV, as summarized in Table 1. As Fe was not detected we assume that the electrodeposited particles are covered by the NCNTs on the Ti substrate.

The corresponding XPS high-resolution C 1s, N 1s, and O 1s spectra are shown in Figure 5. The C 1s spectra can be fitted with four peaks at 284.5 eV, 285.9 eV, 287.2 eV, and 288.7 eV, which can be assigned to C=C, C=N or C–O, C=O or C–N, and N–C=O species.[1b] The four peaks observed in the N 1s spectra at 398.7, 400.0, 401.6, and 403.3 eV are commonly ascribed to pyridinic N, pyrrolic N, graphitic N (g-N), and oxide N,[19] respectively, while the high-resolution spectrum of O 1s with peaks at 530.0 eV, 531.9 eV, and 533.1 eV indicate the presence

of C=O or Ti–O,[20] C–O–C, and C–O–H or N–O species.[21] Since no oxygen is present during NCNT synthesis, it may be assumed that oxygen functional groups form post synthesis during handling of the NCNT composites in air. It is worth noting that a relatively high amount of graphitic N can be found in the synthesised NCNTs over Ti substrates, which may be attributed to the low synthesis temperature of 600 °C. Table 2 summarizes the surface atomic composition of the individual nitrogen species.

In general, the structural characterization in this chapter proves the successful and homogeneous growth of dense layers of NCNTs over Fe particles electrodeposited on Ti foil and Ti mesh.

The electrochemical behaviour of NCNTs@Ti towards the V (IV)/V(V) redox pair, which is one relevant reaction in a VRFB, was analysed by cyclic voltammetry. Figure 6 compares the voltammograms of both NCNTs@Ti foil and NCNTs@Ti mesh for different deposition times of iron as well as different NCNT growth times. The anodic peaks at about 0.5 V vs MSE correspond to the oxidation VO^{2+}, while the cathodic peaks at about 0.3 V vs MSE can be assigned to the reduction of VO_2^+. The redox peaks at ca. 0.03 V vs MSE and −0.1 V vs MSE shown in Figures 6 (b) and (d), respectively, correspond to the V(III)V (IV) redox couple.[9a,22] This redox couple is not of relevance in a running VRFB and will not be discussed further in this study. However, a pronounced V(III)/V(IV) redox activity might be helpful for the initial pre-charging process when applying commercial electrolytes typically containing a V(III):V(IV) ratio of 1:1 as vanadium source in the VRFB.

Peak current density (j_{pa} and j_{pc}), peak potential difference (ΔE_p), as well as the redox onset potentials are a common measure to estimate the catalytic activity of electrode materials.[9b,23] However, on the other hand it has recently been shown, that at least in case of porous electrodes, these values may not necessarily reflect activity, but may also be influenced by porosity, surface area, double layer capacity, etc..[1b,24] To overcome this challenge, we have recently developed an SECM (scanning electrochemical microscope) procedure,[9c] which however is difficult to apply to the present 3-dimensional samples. Thus we restrict ourselves to a qualitative discussion of

Table 2. Fraction of N species related to total N content in NCNTs grown on Ti foil and Ti mesh as determined from XPS characterization.

Relative N content [at%]	Pyridinic-N	Pyrrolic-N	Graphitic-N	N-Oxide
Ti foil	25.3	21.9	46.5	6.3
Ti mesh	28.9	13.0	51.5	6.6

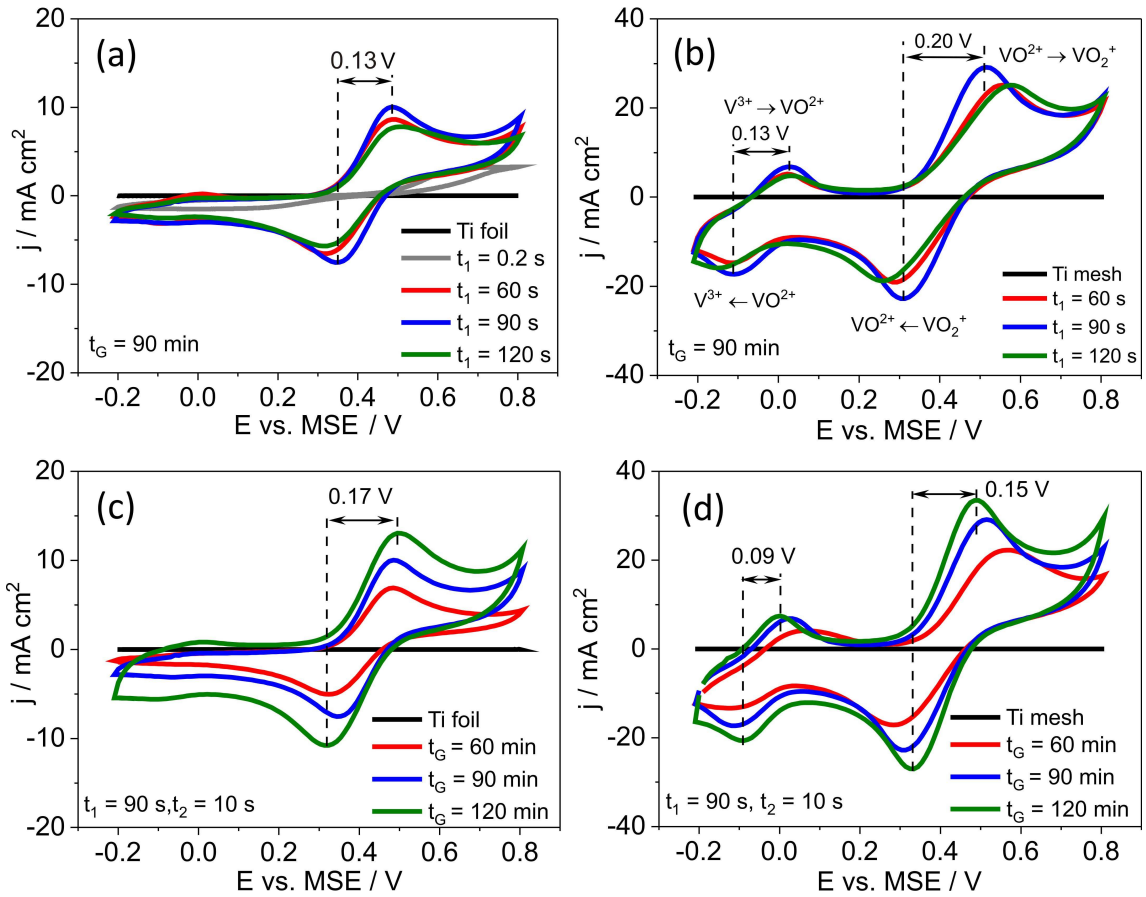

Figure 6. Electrochemical properties of NCNTs on Ti foil and Ti mesh with a scan rate of 50 mVs^{-1}. The fifth cycle is recorded. a) Ti foil and b) Ti mesh substrates showing the effect of various nucleation times, $t_2 = 10$ s, $t_G = 90$ min. c) Ti foil and d) Ti mesh substrates showing the effect of t_G, $T_S = 600$ °C, $t_1 = 90$ s, $t_2 = 10$ s.

the electrochemical results. First of all, from Figure 6 it is obvious that neither Ti foil nor Ti mesh provides significant redox activity towards the V(IV)/V(V) redox pair, making them suitable substrates for the investigation of carbon-based materials towards the given reaction. Moreover, in the case of NCNTs@Ti foil, the values of ΔE_p are 0.16, 0.13 and 0.19 V vs MSE when t_1 was set to 60, 90, and 120 s, respectively, while in the case of NCNTs@Ti mesh, the values of ΔE_p are 0.28, 0.20, and 0.33 V vs MSE, demonstrating that the prepared electrodes provide good redox activity. These promising results are not only superior to those obtained with graphene-nanowall-modified carbon felt (lowest $\Delta E_p = 0.339$ V),[8] but also they are close to the best previously published results obtained on a carbon nanofiber/nanotube (CNF/CNT) composite catalysts grown on carbon felt (CNF/CNT-700, lowest $\Delta E_p = 136.12$ mV) as active electrode material in a VRFB.[25] A slight influence of the iron deposition time is observed with 90 s in both cases as shown in Figures 6 (a) and (b), providing the highest current densities and the lowest peak potential differences. This is in agreement with the results from characterisation, where these samples showed dense coverage with NCNTs but no overgrowth. We assume that the fact that the peak separation in case of Ti foil is smaller does not indicate higher catalytic activity but is due to the highly porous nature of the Ti mesh, thus diffusion within the porous network becomes relevant for CV shape. Accordingly, owing to the three-dimensional structure of the Ti mesh, a three-fold current density (related to geometrical surface area) was achieved compared to the Ti foil.

In Figures 6c and 6d, the cyclic voltammograms of the various samples prepared at different CVD growth times are summarised, exhibiting an increase in peak current densities with growth time and, in case of the Ti mesh, a decrease in the ΔE_p value, which is different to the Ti foil, where a slight increase in peak separation is observed. Again, we would like to point out, that peak separation at porous electrodes is a weak measure for activity and influenced by many parameters such as pore size, inner surface area etc..[26] Since the diffusion profile on a flat substrate (Ti foil) with deposited CNTs will be different to a porous substrate (Ti mesh), there will be different influences on peak separation. The enhancement in current densities is attributed to the increase in the thickness of the NCNT layers on the Ti surface, as shown in Figure 2(g–i) and (j–l). The best performance was obtained on NCNTs@Ti mesh at t_G of 120 min, with the highest j_{pa} and j_{pc}, the lowest ΔE_p value (0.15 V vs MSE), indicating promising activity toward the VO^{2+}/VO_2^+ redox couple of VRFB. In general, it seems that longer NCNT growth times, i.e. thicker NCNT layers, are beneficial for high activity of the composite electrodes. However, it has to be kept in mind that the conditions of testing the electrodes in a half cell are different from those of working VRFB and electrode optimization under realistic conditions has to be done in the future.

Recently, there has been a debate as to which surface structural features in carbon materials form the active sites for redox ion conversion. We have shown that oxygen functional groups seem not to be directly involved but the increased hydrophilicity introduced by them leads to increased wetting and thus to enhanced accessibility of the surface for vanadium redox species.[1b,9a] Accordingly, nitrogen doping may influence the surface properties of the 3-dimensional electrodes leading to complete wetting and good activity.

3. Conclusions

In this study, Ti foil and Ti mesh were investigated as substrates for composite electrodes for VRFB. NCNTs were grown over electrodeposited Fe on these substrates via atmospheric pressure chemical vapor deposition. Optimum parameters for electrodeposition of Fe as well as for growth of NCNTs were established, however, the variation between the properties of the individual samples was moderate. Both NCNTs on Ti foils and Ti mesh show promising redox activity for the VO^{2+}/VO_2^+ redox couple with the highest peak current (about 35 mA cm^{-1}) and the lowest ΔE_p value (0.15 V) for NCNTs@Ti-mesh composite. In general, it is demonstrated that Ti is a suitable substrate electrode material for VRFBs and other electrochemical applications. Furthermore, given the inactivity of this material, it may also be used to study the activity of a catalyst without interference from the substrate. To the best of our knowledge, this is the first report on Ti-based electrodes towards the VO^{2+}/VO_2^+ redox couple for VRFB.

Experimental Section

Electrodeposition of Fe particles was carried out in a plating bath containing $FeSO_4 \cdot 7H_2O$ (0.01 M), Na_2SO_4 (0.1 M), and L-(+)-Ascorbic acid (0.3 M), in a three-electrode setup using pristine annealed Ti foil (Alfa) or Ti mesh (99.8%, pore diameter: 180 μm, wire diameter: 100 μm, OFOLAN, China) with a size of 1×1 cm^2 as the working electrode (WE). A saturated calomel electrode (SCE) was used as reference electrode (RE) and a Pt mesh as counter electrode (CE) at 25 ± 3 °C. Initially, iron deposition was attempted by double pulse deposition, as reported in.[28] However, it turned out that this approach did not yield satisfactory results, probably due to the nature of the Ti substrate, which seems to be covered by a small oxidic layer. Thus, a potential program as shown in Figure 1a was established in a series of experiments, and justified by the fact that beneficial results were obtained. After Fe deposition, the Ti support decorated with Fe particles was placed into an APCVD (atmospheric pressure CVD) reactor and the quartz reactor tube (outer diameter, ca. 33.5 mm) inserted in an oven (Carbolite, Neuhausen, Germany) was purged with argon (Ar) flowing at 50 sccm for about 30 min. Further, the temperature of the growth chamber was ramped up to 600 °C under a gas flow rate of Ar:H_2 = 50 sccm:50 sccm and kept there for 30 min. During the following growth step, the gas was saturated with acetonitrile (ACN) using a bubbler at 30 °C. Finally, the system was cooled down under 50 sccm Ar after the specified growth time as detailed in the results and discussion section.

The electrochemical performance of the prepared NCNTs@Ti composite electrodes toward the positive redox reaction of the vanadium RFB (i.e., the VO^{2+}/VO_2^+ redox couple) was studied by cyclic voltammetry (CV). CV was carried out in a standard three-electrode cell containing 50 mL of 0.1 M vanadium (IV) solution in a 3 M sulfuric acid using an Autolab potentiostat/galvanostat PGstat 302 (Eco Chemie Netherlands). CVs were obtained with a sweep rate of 50 mV s^{-1} at room temperature. The NCNTs@Ti composite

served as the WE, and the area of both NCNTs@Ti foil and NCNTs@Ti mesh were 1×1 cm^2. The CE was a Pt mesh, and the RE was a saturated mercury sulfate electrode ($Hg|HgSO_4|K_2SO_{4(sat.)}$, MSE).

Raman spectra were recorded on a Renishaw InVia instrument using a Cobolt CW DPPS laser (532 nm excitation wavelength), a Peltier cooled charge coupled device detector (CCD) with a grating of 1800 l mm^{-1} and a microscope (Leica, x100 objective). To evaluate the homogeneity of the samples, a Raman mapping experiment was performed using an x-y stage (Prior, 100 nm resolution) in 500 nm steps scanning areas of 10×10 μm^2.

X-ray photoelectron spectroscopy (XPS) was performed using monochromatic Al Kα radiation as the excitation source. Survey spectra in a wide binding energy range were recorded with a step size of 1 eV, while high-resolution spectra for C 1s, N 1s, and O 1s were measured with a step size of 0.1 eV and a dwell time of 50 ms accumulating 50 scans to achieve a reasonable signal-to-noise ratio.

The morphology of electrodeposited Fe particles as well as of NCNTs@Ti was investigated via scanning electron microscopy (SEM) using an ESEM XI 30 FEG (PHILIPS, Germany). The energy-dispersive X-ray spectroscopy (EDX) measurements were performed using an Octane elite plus detector. The measurement conditions were 5 kV accelerating voltage and 50 s measurement time (live time).

Acknowledgements

The authors are indebted to Frank Syrowatka for SEM and EDX measurements and acknowledge funding through the Chinese Scholarship Council CSC.

Keywords: all-vanadium redox flow battery · nitrogen-doped carbon nanotubes · CVD · titanium · nanostructured electrode

[1] a) P. Leung, X. Li, C. Ponce de León, L. Berlouis, C. T. J. Low, F. C. Walsh, *RSC Adv.* **2012**, *2*, 10125–10156; b) S. Rummler, M. Steimecke, S. Schimpf, M. Hartmann, S. Forster, M. Bron, *J. Electrochem. Soc.* **2018**, *165*, A2510-A2518.

[2] a) M. Rychcik, M. Skyllas-Kazacos, *J. Power Sources* **1988**, *22*, 59–67; b) F. Rahman, M. Skyllas-Kazacos, *J. Power Sources* **2009**, *189*, 1212–1219.

[3] a) C. Ding, H. Zhang, X. Li, T. Liu, F. Xing, *J. Phys. Chem. Lett.* **2013**, *4*, 1281–1294; b) M. Park, J. Ryu, J. Cho, *Chem. Asian J.* **2015**, *10*, 2096–2110.

[4] D. S. Aaron, Q. Liu, Z. Tang, G. M. Grim, A. B. Papandrew, A. Turhan, T. A. Zawodzinski, M. M. Mench, *J. Power Sources* **2012**, *206*, 450–453.

[5] T. M. Tseng, R. H. Huang, C. Y. Huang, C. C. Liu, K. L. Hsueh, F. S. Shieu, *J. Electrochem. Soc.* **2014**, *161*, A1132-A1138.

[6] a) K. J. Kim, M. S. Park, Y. J. Kim, J. H. Kim, S. X. Dou, M. Skyllas-Kazacos, *J. Mater. Chem. A* **2015**, *3*, 16913–16933; b) Z. González, C. Botas, C. Blanco, R. Santamaría, M. Granda, P. Álvarez, R. Menéndez, *Nano Energy* **2013**, *2*, 1322–1328.

[7] Y. Kim, Y. Y. Choi, N. Yun, M. Yang, Y. Jeon, K. J. Kim, J.-I. Choi, *J. Power Sources* **2018**, *408*, 128–135.

[8] W. Li, Z. Zhang, Y. Tang, H. Bian, T. W. Ng, W. Zhang, C. S. Lee, *Adv. Sci.* **2016**, *3*, 1500276–1500283.

[9] a) M. Steimecke, S. Rummler, N.-F. Schuhmacher, T. Lindenberg, M. Hartmann, M. Bron, *Electroanalysis* **2017**, *29*, 1056–1061; b) C. Noh, S. Moon, Y. Chung, Y. Kwon, *J. Mater. Chem. A* **2017**, *5*, 21334–21342; c) M. Steimecke, S. Rümmler, M. Kühhirt, M. Bron, *ChemElectroChem* **2016**, *3*, 318–322.

[10] J. Melke, P. Jakes, J. Langner, L. Riekehr, U. Kunz, Z. Zhao Karger, A. Nefedov, H. Sezen, C. Wöll, H. Ehrenberg, C. Roth, *Carbon* **2014**, *78*, 220–230.

[11] L. Wu, Y. Shen, L. Yu, J. Xi, X. Qiu, *Nano Energy* **2016**, *28*, 19–28.

[12] L. D. Brown, T. P. Neville, R. Jervis, T. J. Mason, P. R. Shearing, D. J. L. Brett, *J. Energy Storage* **2016**, *8*, 91–98.

[13] a) L. F. Arenas, C. Ponce de León, F. C. Walsh, *Curr. Opin. Electrochemistry* **2019**, *16*, 1–9; b) H. Zhang, J. M. de Souza e Silva, X. Lu, C. S. de Oliveira, B. Cui, X. Li, C. Lin, S. L. Schweizer, A. W. Maijenburg, M. Bron, R. B. Wehrspohn, *Adv. Mater. Interfaces* **2019**, *6*.

[14] H. J. Liu, T. T. Cai, Q. S. Song, L. X. Yang, Q. Xu, C. W. Yan, *Int. J. Electrochem. Sci.* **2013**, *8*, 2515–2523.

[15] a) P. Wang, T. Kottakkat, M. Bron, *ChemElectroChem* **2015**, *2*, 1396–1402; b) S. Kundu, T. C. Nagaiah, X. Chen, W. Xia, M. Bron, W. Schuhmann, M. Muhler, *Carbon* **2012**, *50*, 4534–4542.

[16] a) X. Li, W. Cai, J. An, S. Kim, J. Nah, D. Yang, R. Piner, A. Velamakanni, I. Jung, E. Tutuc, S. K. Banerjee, L. Colombo, R. S. Ruoff, *Science* **2009**, *324*, 1312–1314; b) I. Vlassiouk, S. Smirnov, M. Regmi, S. P. Surwade, N. Srivastava, R. Feenstra, G. Eres, C. Parish, N. Lavrik, P. Datskos, S. Dai, P. Fulvio, *J. Phys. Chem. C* **2013**, *117*, 18919–18926.

[17] L. L. Patera, F. Bianchini, C. Africh, C. Dri, G. Soldano, M. M. Mariscal, M. Peressi, G. Comelli, *Science* **2018**, *359*, 1243–1246.

[18] Y. Xue, B. Wu, Y. Guo, L. Huang, L. Jiang, J. Chen, D. Geng, Y. Liu, W. Hu, G. Yu, *Nano Res.* **2011**, *4*, 1208–1214.

[19] a) Y. Zhong, M. Jaidann, Y. Zhang, G. Zhang, H. Liu, M. Ioan Ionescu, R. Li, X. Sun, H. Abou Rachid, L. S. Lussier, *J. Phys. Chem. Solids* **2010**, *71*, 134–139; b) Z. Chen, D. Higgins, Z. Chen, *Carbon* **2010**, *48*, 3057–3065.

[20] C. H. Kim, B.-H. Kim, K. S. Yang, *Carbon* **2012**, *50*, 2472–2481.

[21] a) Y. K. Kim, H. Park, *Energy Environ. Sci.* **2011**, *4*, 685–694; b) S. Wu, G. Wen, J. Wang, J. Rong, B. Zong, R. Schlögl, D. S. Su, *Catal. Sci. Technol.* **2014**, *4*, 4183–4187.

[22] H.-S. Kim, *Bull. Korean Chem. Soc.* **2011**, *32*, 571–575.

[23] L. Eifert, Z. Jusys, R. Banerjee, R. J. Behm, R. Zeis, *ACS Appl. Energy Mater.* **2018**, *1*, 6714–6718.

[24] M. Steimecke, S. Rümmler, M. Bron, *Electrochim. Acta* **2015**, *163*, 1–8.

[25] M. Park, Y. J. Jung, J. Kim, H. Lee, J. Cho, *Nano Lett.* **2013**, *13*, 4833–4839.

[26] a) D. Menshykau, R. G. Compton, *Electroanalysis* **2008**, *20*, 2387–2394; b) C. Punckt, M. A. Pope, I. A. Aksay, *J. Phys. Chem. C* **2013**, *117*, 16076–16086.

[27] W. Zhang, J. Xi, Z. Li, H. Zhou, L. Liu, Z. Wu, X. Qiu, *Electrochim. Acta* **2013**, *89*, 429–435.

[28] M. Uedaa, H. Dietz, A. Anders, H. Kneppe, A. Meixner, W. Plieth, *Electrochim. Acta* **2002**, *48*, 377–386.

Manuscript received: November 11, 2019
Revised manuscript received: December 18, 2019
Accepted manuscript online: January 2, 2020